CFD Investigation of the test facility for forced blade flutter research

Jindřich Hála[1*], *Jan* Lepičovský[1], *Petr* Šidlof[2], and *David* Šimurda[1]

[1]Institute of Thermomechanics of the Czech Academy of Sciences, Dolejškova 1402/5, 182 00, Prague 8, Czech Republic
[2]Technical University of Liberec, Studentská 1402/2, 461 17, Liberec, Czech Republic

Abstract. With the increasing share of renewable power resources turbomachines need to be operated under a wider range of operating conditions including highly off-design regimes. Under such regimes an undesirable phenomenon of blade flutter might occur and possibly destroy the machine. To prevent this, intensive research is conducted by research teams worldwide. Blade flutter research program at the Institute of Thermomechanics of the Czech academy of sciences (IT CAS) mainly aims to advance experimental techniques for investigation of sonic and transonic blade flutter. For this purpose, the new sophisticated test facility was designed and manufactured. As part of the design process, the CFD computations were conducted in order to investigate the flow field in the test facility. This paper presents results of these computations with detailed analysis of flow structures occurring during the air flow through the stationary blade cascade.

1 Introduction

Recently a test section for investigation of forced oscillation of blades in a compressor blade cascade operating at transonic regimes has been designed in frame of a cooperation between the Institute of Thermomechanics of the Czech Academy of Sciences (IT CAS) and Technical University of Liberec (TUL) [1]. The test section is mounted on the modular in-draft wind tunnel (Fig. 1) stationed at Aerodynamic Laboratory in Nový Knín. The tunnel facility (Fig. 2) consists of a silica gel dryer (1), bell mouth inlet (2) with honeycomb flow straighteners (3), round-rectangular transition (4), flutter test facility with tested blade cascade (5), outlet part equipped with control nozzle (6) and fast acting gate valve (7) connected to a vacuum tank. The flow in the cascade is controlled using adjustable tailbords, throttling tailboard and regulating nozzle. The tested blades can be independently oscillated and a resulting flow field and mutual interaction between blades can be measured using numerous techniques including fast-response miniature pressure transducers, pressure sensitive paints, fibre optics interferometry, thermo-anemometer probes and high-speed torquemeter.Due to only slightly supersonic inlet velocity and limited space at the test section upper wall, it was decided that the inlet channel would be straight with no divergence. Preliminary tests would be run and according to the results of the first tests, a suction through the upper wall will be added to suppress reflection of shock waves back to the

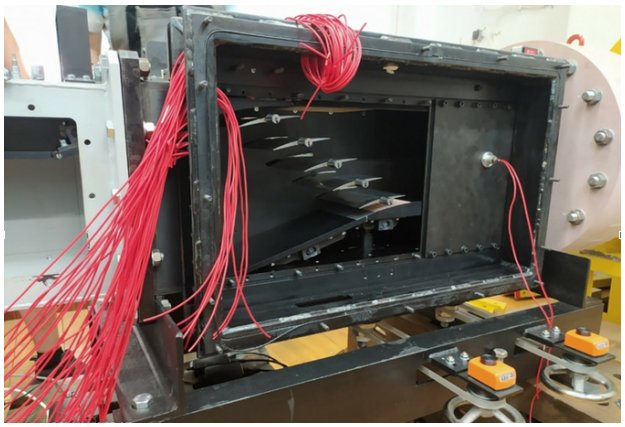

Fig. 1. Test section with uncovered side wall and visible blade cascade (flow direction from right to left).

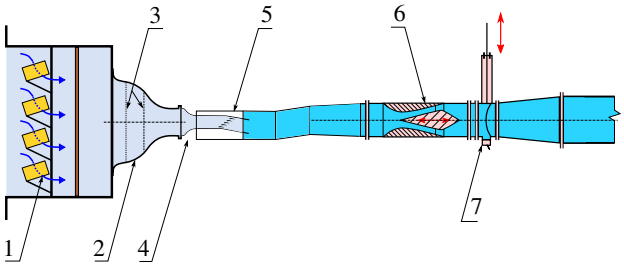

Fig. 2. Schematic depiction of the modular wind tunnel with the mounted flutter test facility.

*Corresponding author: hala@it.cas.cz

flow and also to allow for acceleration to higher inlet Mach numbers if necessary.

The aim of this work was to investigate the flow field in the test section using readily available numerical techniques represented by Ansys Fluent commercial code and provide numerical data for the initial stage of measurements. This work did not aim to investigate interaction between oscillating blades, thus, only stationary cascade was considered. Further sections briefly introduce numerical techniques used throughout this investigation including numerical grid and provide thorough analysis of the flow in the test section based on the obtained results.

2 Investigated blade cascade

Blade cascade represents a section of a fan rotor at 45% span. It has design inlet Mach number $M_1 = 1.09$, design inlet flow angle 148.5° and design flow turning 12.5°. Further details can be found in [2]. This cascade has been chosen since blades are reasonably thick to allow unchallenging instrumentation with Kulite fast response pressure transducers and also because data on its performance are available in the open literature.

3 Numerical simulation

The problem was numerically modelled in 3D using the system of time-averaged Navier-Stokes equations for compressible flows:

$$\frac{\partial \rho}{\partial t} + \frac{\partial \left(\rho u_j\right)}{\partial x_j} = 0, \tag{1}$$

$$\frac{\partial \left(\rho u_i\right)}{\partial t} + \frac{\partial \left(\rho u_i u_j\right)}{\partial x_j} = -\frac{\partial p}{\partial x_i} + \frac{\partial \tau_{ij}^{\text{eff.}}}{\partial x_j}, \tag{2}$$

$$\frac{\partial \left(\rho e_0\right)}{\partial t} + \frac{\partial \left(\rho h_0 u_j\right)}{\partial x_j} = \frac{\partial}{\partial x_j}\left(\tau_{ij}^{\text{eff.}} u_i + \rho \alpha^{\text{eff.}} \frac{\partial h}{\partial x_j}\right), \tag{3}$$

Since the flow medium is dry air, the equation of state of an ideal gas was considered. The Reynolds stress tensor and the turbulent thermal diffusivity were computed using k − ω SST turbulence model.

The inviscid fluxes were approximated using the Advection Upstream Splitting Method (AUSM) upwind scheme with linear reconstruction. The steady state solution was obtained using the density-based implicit solver in Ansys Fluent R2021 commercial code employing second order accuracy upwind schemes in space. The computations were conducted using the high performance computing cluster of the Institute of Thermomechanics using 16 cores of the *Intel Xeon E5-2683 v4* processor running at 2.10 GHz.

3.1 Computational domain and grid

The investigated cascade consists of five transonic profiles placed in the cascade with a chord length of $c = 120$ mm pitch $t = 74.52$ mm and stagger angle $\gamma = -41.49°$. To capture the effect of boundary layer growth inside the bell-mouth contraction and of the possible corner vortex formation in the round-rectangular transition upstream the cascade, the entire inlet part was included in the simulation. The computational domain can be seen in Fig. 3.

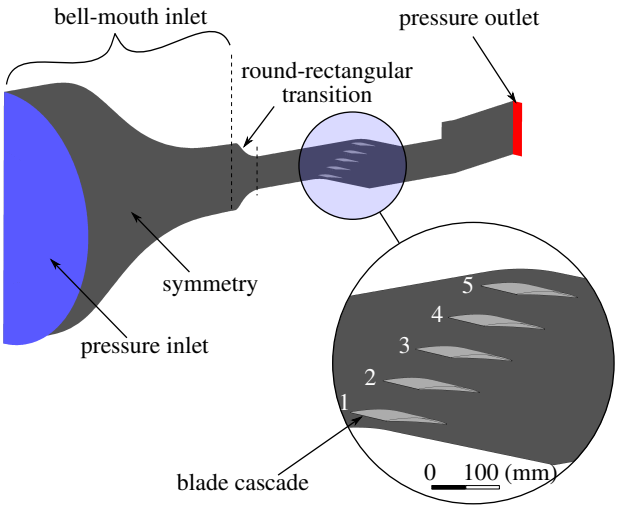

Fig. 3. Computational domain with the detail of the cas-cade and marked blade numbers.

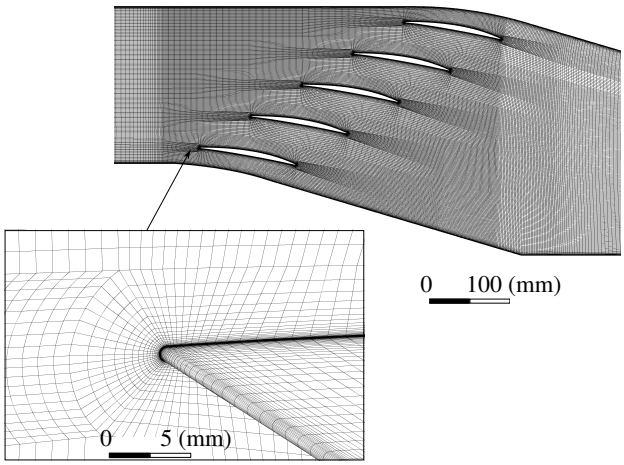

Fig. 4. Computational grid around the cascade and the detail of the blade – end wall transition close to a blade leading edge.

The computational grid consists of approximately $15 \cdot 10^6$ hexahedral cells. The dimensionless wall distance y^+ of the first cell at the blade surfaces and test section walls was less then 1 with the cell growth ratio 1.2. Fig. 4 shows the grid around the cascade and the detail of the blade – end wall transition close to a blade leading edge.

3.2 Boundary conditions

The domain is symmetric in the span-wise direction, therefore a symmetry boundary condition was used in the mid plane. At the outlet, the average static pressure of 20 kPa

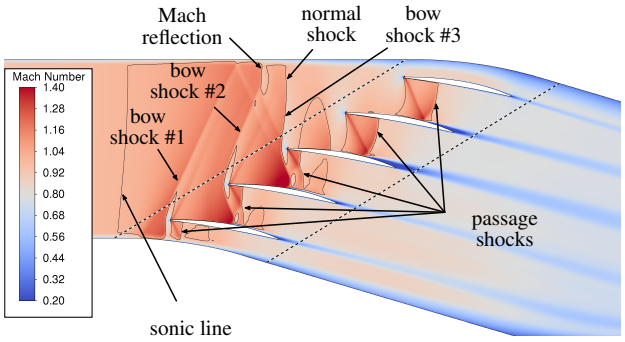

Fig. 5. Mach number contours of the region in the channel mid-plane around the cascade with the marked main flow features.

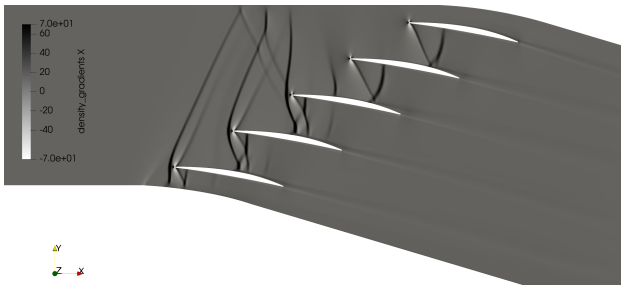

Fig. 6. Contours of the density gradient in x direction $\partial\rho/\partial x$ depicting shock waves in the flow field around the cascade.

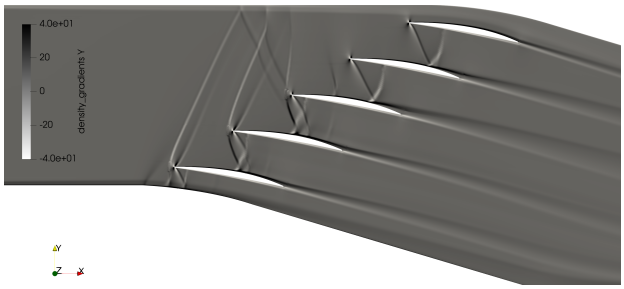

Fig. 7. Contours of the density gradient in y direction $\partial\rho/\partial y$ depicting shock waves and wakes behind blades.

was set. Following boundary conditions were set at the inlet:

1. constant total temperature $T_0 = 300\,\mathrm{K}$
2. uniform total pressure distribution $p_0 = 101.325\,\mathrm{kPa}$
3. constant turbulence intensity $Tu = 2\%$
4. constant turbulent viscosity ratio $\frac{\mu_t}{\mu} = 10$

4 Results and discussion

In reality, blading is annular and thus periodic. Therefore, a turbomachinery cascade modelling aims to model the flow as periodic as possible. This, however, appears to be one of the main difficulties with experimental modelling of transonic flow past finite linear compressor blade cascades. In the current investigation, owing to the setup, the flow is not periodic. Therefore one of the aims of the current investigation is to understand in detail sources of this aperiodicity in order to deal with it as best as possible. Figure 5 shows the Mach number contours around the cascade in the mid-plane with the sonic line in black and dashed lines upstream and downstream the cascade representing the locations in which the static pressure tapping will be located during the experiments.

As the contours of Mach number in Fig. 5 suggest, the flow is accelerated to supersonic velocity just before the cascade at the point where the lower wall becomes divergent (approximately 0.5 chord length before the leading edge of blade No. 1). The Sonic line stretches from this point across the whole inlet channel. This is an aerodynamic throat that determines mass flow through the blade cascade. Inlet flow is supersonic up to the blade No.3. Here, a normal shock knocks the velocity down to subsonic. This is due to interaction of detached bow shock waves #1 and #2 with the upper wall boundary layer. Upon the interaction with the shock wave #1, the boundary layer thickness starts to grow. This leads to such conditions that the interaction with shock wave #2 results in a Mach reflection. It can be seen that the normal shock of this interaction decelerates the flow to subsonic velocity and more importantly causes the boundary layer to rapidly grow in thickness. Subsonic region downstream the normal shock of the Mach reflection is not large and the flow accelerates back to supersonic velocity. Upon passing through the bow shock of the blade No. 3, however, supersonic velocity can not be maintained any more and flow upstream of blades No. 4 and No. 5 becomes subsonic with only a limited supersonic region on the suction surface of blade No. 3, i.e. upstream of the blade No. 4. Due to this configuration the passages in between blades No. 1, 2 and 3 operate at started supersonic inlet flow conditions whereas passages between blades No. 3, 4 and 5 operate at choked flow conditions [3]. This inlet flow aperiodicity is associated not only with the distribution of the inlet Mach number but also with that of the inlet flow angle (see Figs. 8a and 9a). In the region upstream of blades 4 and 5 where the flow is decelerated as described previously, the inlet flow angle drops to lower values towards slightly negative incidence. This results in the increased mass flow rate through these two interblade passages (Tab. 1).

The actual shock wave pattern is more apparent from Fig. 6 and 7 which shows the contours of density gradients in x and y direction respectively. Such contours mimic schlieren technique which is commonly used for shock wave visualisation in compressible flow research. The wakes behind the cascade which are nearly perpendicular to y axis can be better seen in Fig. 7. The darker regions then show compression in x and y direction, while the bright regions show expansion in these directions. It can be seen from Fig. 7 that thickness of the wakes is determined by the strength and position of the passage shock

Table 1: Mass flow rate through the individual inter-blade passages.

Passage number	**Mass flow rate** $\left(\mathrm{kg}\cdot\mathrm{s}^{-1}\right)$	**Mass flux** $\left(\mathrm{kg}\cdot\mathrm{s}^{-1}\cdot\mathrm{m}^{-2}\right)$
6	0.223	77.81
5	0.761	129.05
4	0.769	130.44
3	0.732	124.12
2	0.742	125.84
1	0.381	126.41

wave in each inter-blade channel. The least favourable situation is in between blades 3-4 and 4-5. Here, the passage shock wave interacts with the suction side of blades 3 and 4 exactly at the point where the inter-blade channel starts to be divergent and the boundary layer is subject to adverse pressure gradient not mentioning the shock wave. Therefore Local flow separation takes place and the wake is wide. Situation in the inter-blade channel 3-4 is even more serious than in 4-5 since the passage shock wave is stronger there. This results also in distinct peaks in the distribution of the exit flow angle in F ig. 8b downstream of blades 3 and 4.

The qualitative difference between supersonic inlet flow conditions and choked flow conditions at the inlet to individual inter-blade passages is the principal cause of the flow field aperiodicity. As can be seen in Table 1, the mass flux through all the passages is nearly equal except the passage #6 (passage above the upper blade) in which case the mass flux is at approximately 60% compared to other passages. This is most likely due to the presence of the thick boundary layer at the upper wall of the test section. The increase in thickness is caused by already described successive interaction with the three shock waves.

5 Conclusions

The CFD computations of the new test section for investigation of the forced blade oscillations allowed to uncover the main flow features that might be expected during the experiments. The sources of flow aperiodicity, which represents one of the main concerns in the linear blade cascade investigation, were successfully identified in the form of shock wave-boundary layer interaction at the upper wall of the test section. It can be concluded that the planned installation of the upper wall suction should effectively mitigate the adverse effects of this interaction on flow periodicity and provide additional control to control the inlet Mach number. Further CFD simulations of the new test section will be focused on the simulation of the upper wall suction and the effect of the middle blade rotation on the forces acting on the other blades in the cascade.

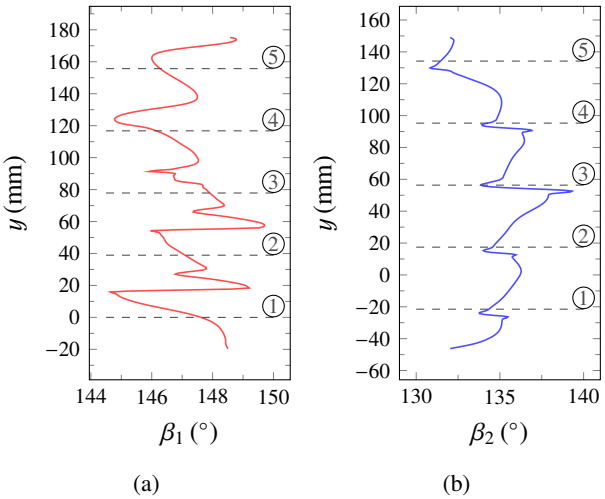

Fig. 8. Flow angle β_1 in the plane in the normal distance of 15mm upstream the cascade (a) and β_2 in the plane 15mm downstream the cascade (b).

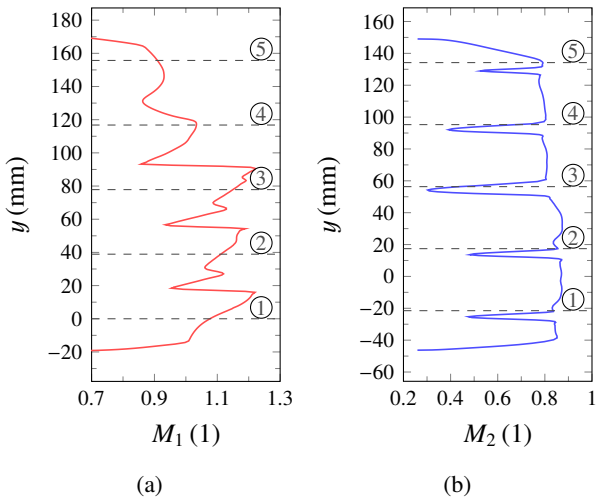

Fig. 9. Mach number in the plane in the normal distance of 15mm upstream the cascade (a) and in the plane 15mm downstream the cascade (b).

This research was supported by the Ministry of Education, Youth and Sports of the Czech Republic – program Inter-Excellence, project No. LTAUSA19036. Institu-tional support RVO:61388998 of the Institute of Thermomechan-ics of the Czech Academy of Sciences is also acknowledged.

References

[1] J. Lepičovský, P. Šidlof, D. Šimurda, M. Štěpán, M. Luxa, AIP Conference Proceedings **2323**, 030001 (2021)

[2] H. A. Schreiber, H. Starken, ASME J. Eng. Gas Turbines Power **106(2)**, 288-294 (1984)

[3] H. J. Lichtfuss, H. Starken, Progress in Aerospace Sciences **15**, 37-149 (1974)